OLEDs Based on the Emission of Interface and Bulk Exciplexes Formed by Cyano-Substituted Carbazole Derivative

Eigirdas Skuodis, Ausra Tomkeviciene, Renji Reghu, Laura Peciulyte, Khrystyna Ivaniuk, Dmytro Volyniuk, Oleksandr Bezvikonnyi, Gintautas Bagdziunas, Dalius Gudeika, Juozas V. Grazulevicius

Department of Polymer Chemistry and Technology, Kaunas University of Technology, Radvilenu Plentas 19, LT-50254 Kaunas, Lithuania; e-mail: juozas.grazulevicius@ktu.lt

Abstract: Four carbazol-9-yl and diphenylamino substituted 9-ethylcarbazole derivatives having cyano groups in the substituents were synthesized and characterized by the experimental and theoretical tools. Thermal, optical, photophysical and electrochemical properties were studied. The derivatives exhibited moderate thermal stability with 5 % weight loss temperatures exceeding 300^{o}C. All the derivatives were found to be capable of glass formation with glass transition temperatures ranging from 77 to 111 ^{o}C. The optical band gaps of the solid samples were 2.84–3.38 eV. One of the derivatives was used for the preparation of blue non-doped emitting layer and as exciplex forming material for the fabrication of blue and yellow organic light emitting diodes with CIE color coordinates of (0.17, 0.28) and (0.40, 0.52), respectively. The electroluminescence of the yellow exciplexes based device resulted from the overlapping of sky blue bulk emission with photoluminescence quantum efficiency of 43.8% and orange interface exciplex emission with the efficiency of 3.84%. The fluorescent non-doped blue OLED exhibited maximum luminance of 2515 cd/m^2 and external quantum efficiency reaching of 2 %, while the yellow exciplex OLED exploiting the effect of thermally activated delayed fluorescence had maximum luminance of

6260 cd/m^2 and external quantum efficiency of 5.8 %. In addition, sky-blue and orange OLEDs with only one exciplex-based emitter were fabricated showing external quantum efficiencies of 4.2 and 3.2 %, respectively. This work provides background for the fabrication of efficient OLEDs combining advantages of both interface and bulk exciplex emissions (maximal internal quantum efficiency of 100%, provision of exelent charge balance in emitting layer, formation of the "active" planar pn heterojunctions).

Keywords: Carbazole, cyano groups, organic light emitting diode, exciplex, delayed fluorescence.

---

1. Introduction

Organic light-emitting diodes (OLEDs) based on thermally activated delayed fluorescence (TADF) emitters are promising devices for display and illumination technologies [1, 2]. Utilizing TADF emitters, maximum internal quantum efficiencies (100%) can be obtained in florescencent OLEDs by harvesting both singlet and triplet excitons through the reverse intersystem crossing (RISC) [3]. Possibility of the full harvesting of the both singlet and triplet excitons in organic materials for OLED applications was firstly discovered in heavy metal-based phosphorescent emitters [4]. However, TADF emitters are nowadays at the very forefront of materials science because of their advantages over phosphorescent emitters such as absence of rare and high cost heavy metals, wide range of emitting colors, environmental benignity ect [5]. Utilizing TADF emitters, all-color high-efficient OLEDs with maximal internal quantum efficiency (IQE) close to 100% and with maximal external quantum efficiency (EQE) close to 30% were recently develop [3,6]. Moreover, owing to strongly horizontally oriented emitting dipoles of TADF emitters that rises the optical outcoupling/extraction efficiency of OLEDs, maximal EQE of 37% was obtained

without additional out-coupling [5]. Owing the spatial overlap between the highest occupied molecular orbital (HOMO) and the lowest unoccupied molecular orbital (LUMO) in materials containing electron donating and accepting units, the TADF can be obtained due to the negligibly small singlet–triplet energy splitting (ΔE_{ST}) which leads to up-conversion of the lowest excited triplet (T_1) states to the emissive singlet (S_1) state [5,7,8]. Appart from the molecular TADF emitters, the synthetizis of which usually is not trivial [6], TADF can be achieved in simple solid state mixtures of two donor and acceptor materials, forming exciplexes S_1 and T_1 states of which are very close what can lead to reverse intersystem crossing (RISC) [9,10]. Therefore, maximal IQE of 100% can also be achieved in OLEDs based on the exciplex emitters [11]. For achieving maximal IQE of 100%, exciplex systems having almost no any non-radiative processes of triplet exciplexes are required [11]. This challenge stimulates the search for new more effective TADF exciplex-forming materials. In addition, exciplex forming molecular mixtures were proposed as efficient hosts for TADF and phosphorescent OLEDs with improved performance compared to that of the devices based on the conventional molecular hosts [12,13].

Exciplexes can be formed between two different molecules being in a single layer and in two different layers of depending on OLED architecture [14,15]. Both interface and bulk exciplexes were utilized as emitters or hosts in OLEDs [16,17,18]. The interface exciplexes can be utilized not only as TADF emitters but also as active planar pn heterojunctions, which dramatically reduce turn-on voltage of OLEDs [19]. The interface exciplexes were shown to be more efficient hosts than bulk exciplexes for stable and efficient orange phosphorescence OLEDs with low efficiency roll-off and long lifetime [20]. Electroluminescence of OLEDs can also consit of the combination of interface exciplex emission and of monomer emission [21]. On the other hand, exploitation of bulk exciplexes enables to provide the charge balance in emitting layers of efficient exciplex-based OLEDs [22].

Thus previously reports on exciplex-based OLEDs disclose advantages of both interface and bulk exciplexes which were used separately in the devices.

In this work, we developed OLEDs based on both interface and bulk exciplex emission exploiting new carbazolyl substituted derivative containing cyano groups. The results obtained show that exploitation of of both interface and bulk exciplexes in OLED allows not only to increase its efficiency but also to change the color of electroluminescence. Since CIE chromaticity coordinates of electroluminescence of the known exciplex-based OLEDs are still far from the National Television System Committee (NTSC) color standards [23], this our finding can be useful for the monitoring of electroluminescence color. In order to estimate the applicability in OLEDs, the thermal, photophysical electrochemical and photoelectrical properties of the differently substituted carbazole based derivatives with electron-accepting cyano substitutes were studied. Exciplex-based TADF was identified for the molecular mixtures of the newly synthesized cyano substituted carbazole derivative with tris(4-carbazoyl-9-ylphenyl)amine (TCTA) and 4,4′,4″-tris[3-methylphenyl(phenyl)amino]triphenylamine (m-MTDATA). This finding allowed us to develop a new approach for the fabrication of effective OLEDs in wich both interface and bulk exciplexes were utilized as emitters. The approach is demonstrated with the example of yellow OLED showing maximum external quantum efficiency (η_{ex}) of 5.8 % which is higher than theoretically possible η_{ex} of fluorescence OLEDs. To our opinion, combinination of the advantages of both interface and bulk exciplex emissions, in the future, can lead to the considerable increase of efficiencies of exciplex-based OLEDs.

2. Experimental

2.1. Instrumentation

^{1}H and ^{13}C NMR spectra were recorded using *Bruker Avance III* [700 MHz (^{1}H), 175 MHz (^{13}C)] spectrometer at room temperature. All the data are given as chemical shifts in δ (ppm), $(CH_3)_4Si$ (TMS, 0 ppm) was used as an internal standard. Infrared (IR) spectra were recorded by *Perkin Elmer Spectrum BX II FT-IR System* spectrometer. The spectra of the solid compounds were recorded using KBr pellets. Mass (MS) spectra were recorded on *a Waters Acquity UPLC* mass spectrometer. Melting points (m.p.) of the synthesized compounds were estimated using *Electrothermal Mel-Temp* melting point apparatus.

Differential scanning calorimetry (DSC) measurements were carried out in a nitrogen atmosphere with a *DSC Q-2000* thermal analyser at a heating rate of 10 ^{o}C/min. Thermogravimetric analysis (TGA) was performed on a *TGA Q-50* aparatus in a nitrogen atmosphere at a heating rate 10 ^{o}C/min. Absorption spectra of the dilute tetrahydrofuran (THF) solutions were recorded on *Perkin Elmer Lambda 35* spectrometer. Room and low (77K) temperature photoluminescence (PL) spectra of the synthesized compounds were investigated by *FLS980* fluorescence spectrometer with *TMS300* monochromators and a red cooled detector (*Hamamatsu R928P*). The standard light source for measuring of PL spectra was a 450 W xenon arc lamp. PL spectra of the samples were recovered at the excitation wavelength of 350 nm and the scan speed of 1 nm/s. For these measurements, the dilute solutions of the investigated compounds were prepared by dissolving them in a spectral grade THF at 10^{-5} M concentration. PL decay curves of the layers of the exciplex forming molecular mixtures and a PL intensity dependence on laser flux were recorded with the *Edinburgh Instruments FLS980* spectrometer at room temperature using a *PicoQuant LDH-D-C-375* laser (wavelength 374 nm) as the excitation source. Variable temperature liquid nitrogen cryostat (Optistat DN2) was used

for the studies of photophysic properties of the samples at different temperatures under inert atmosphere (N_2).

The cyclic voltammetry (CV) measurements were carried out by a three-electrode assembly cell from *Bio-Logic SAS* and a *micro-AUTOLAB Type III* potentiostat-galvanostat. The working electrode was a glassy carbon of 0.12 cm^2 surface although the reference electrode and the counter electrode were Ag/Ag^+ 0.01 M and Pt wire respectively. The solutions with the concentration of 10^{-3} M of the compounds in argon-purged dichloromethane (Fluka) with 0.1M tetrabulthylammonium hexafluorophosphate as electrolyte were used for the CV measurements. At the end of the measurements, ferrocene was added as internal reference.

The ionization potentials (IP_{EP}) of the films of the synthesized compounds were measured by the electron photoemission in air method as reported earlier [24, 25]. The samples for the measurements were prepared by dissolving compounds in THF and by casting on indium tin oxide (ITO) coated glass plates. The experimental setup consisted a deep UV deuterium light source ASBN-D130-CM, a CM110 1/8m monochromator, and an electrometer 6517B Keithley.

The charge carrier mobility (μ) measurements were carried by the time of flight method (TOF) [26, 27]. The sandwich-like cells (ITO/the synthesized compounds/Al) were fabricated for the measurements. The samples for TOF measurements were prepared by vacuum deposition of the compounds on a pre-cleaned glass/ITO substrate and the 60 nm aluminum top electrode. The thickness of the films was measured using method carrier extraction in linearly increasing voltage (CELIV) (ε~3) [28]. The charge carriers were generated at the layer surface by illumination with a pulsed Nd:YAG laser (EKSPLA NL300, a wavelength of 355 nm, pulse duration 3-6 ns). The transit time was determined from the kink point in the transient photocurrent curves. The transit time t_t with the applied bias (V) indicates the passage of holes through the entire thickness of the cell (*d*) and

enables determination of the hole mobility as $\mu=d^2/U\cdot t_t$. The experimental setup was as reported earlier consisting of a *Keithley 6517B* electrometer and a *Tektronix TDS 3052C* oscilloscope [29].

The electroluminescent devices were fabricated by means of vacuum deposition of organic semiconductor layers and metal electrodes onto pre-cleaned ITO coated glass substrate under vacuum of 10^{-6} Torr. The active area of the obtained devices was 6 mm^2. The density-voltage and luminance-voltage characteristics were measured using a *Keithley 6517B* electrometer and a *Keithley 2400C* sourcemeter in air without passivation immediately after the formation of the device. The brightness measurements were done using a calibrated photodiode [30, 31].

2.2. Materials

3-Amino-9-ethylcarbazole and 4-cyanophenyliodide were purchased from Sigma Aldrich, and were used without purification. 3-Iodocarbazole [32], 3,6-diiodocarbazole [32], 3-iodo-9-ethylcarbazole [33], 4-bromo-2‘-nitrobiphenyl[34] 2-bromocarbazole[33] 2-bromo-9-ethylcarbazole,[35] 4,4‘-dibromo-2-nitrobiphenyl [36], 2,7-dibromocarbazole [33], and 2,7-dicyanocarbazole [37], were prepared according to the published procedures.

3-Cyano-9*H*-carbazole. 3-Iodocarbazole (4.50 g, 15.4 mmol), copper (I) cyanide (2.79 g, 30.8 mmol) and N-methyl-2-pyrrolidone (NMP, 50 ml) were mixed in a flask. The reaction mixture was heated at 155 ^oC under nitrogen atmosphere for 22 h. The reaction mixture was then cooled to room temperature and poured into a solution of cold water (500 ml), hydrochloric acid (80 ml) and $FeCl_3$ (16 g). The reaction mixture was heated at 80^oC for 1 h, and then cooled to room temperature. The precipitate which had formed was filtered off. The product was crystallized from methanol and was obtained as light brown crystals (mp = 187–188 ^oC, lit.: 189–190 ^oC [38]) in 30% (0.89 g) yield.

^{1}H NMR (400 MHz, DMSO-d_6) δ (ppm): 10.50 (s, 1H, NH), 7.33 (s, 1H, Ar), 6.87 (d, J = 7.7 Hz, 1H, Ar), 6.38 (d, J = 8.3 Hz, 1H, Ar), 6.26 (d, J = 8.4 Hz, 1H, Ar), 6.20 (d, J = 8.0 Hz, 1H, Ar), 6.11 (t, J = 7.4 Hz, 1H, Ar), 5.88 (t, J = 7.3 Hz, 1H, Ar).

^{13}C NMR (100 MHz, DMSO-d_6) δ (ppm):142.1, 140.7, 129.0, 127.4, 126.0, 123.0, 122.0, 121.4, 121.0, 120.3, 112.4, 112.0, 100.7.

3-Di(4-cyanophenyl)amino-9-ethylcarbazole (1) was obtained by an improved Ullman coupling reaction. 3-Amino-9-ethylcarbazole (0.7g, 3.3 mmol), 4-cyanophenyliodide (3 g, 13.2 mmol), powdered anhydrous potassium carbonate (5.46 g, 39.6 mmol), copper powder (1.47 g, 23 mmol), and 18-crown-6 (0.3 g) were refluxed in *o*-dichlorobenzene (*o*-DCB, 15 ml) under nitrogen atmosphere for 20 h. Then copper and inorganic salts were removed by filtration of the hot reaction mixture. The solvent was distilled under reduced pressure. The product was purified by silica gel column chromatography using hexane/ethylacetate (20/1) as an eluent. The target compound was obtained as light brown crystals (fw = 412 g/mol, mp = 168–171 ^{o}C) in 32% (0.45 g) yield.

^{1}H NMR (400 MHz, DMSO-d_6) δ (ppm): 8.15 (d, J = 7.8 Hz, 1H, Ar), 8.11 (s, 1H, Ar), 7.74 – 7.69 (m, 5H, Ar), 7.65 (d, J = 8.2 Hz, 1H, Ar), 7.48 (t, J = 8.3 Hz, 1H, Ar), 7.30 (dd, J = 8.6 Hz, 2.1 Hz, 1H, Ar), 7.21 – 7.14 (m, 5H, Ar), 4.47 (q, J = 7.1 Hz, 2H, NC$\underline{H}_2$), 1.35 (t, J = 7 Hz, 3H, C$\underline{H}_3$).

^{13}C NMR (100 MHz, DMSO-d_6) δ (ppm): 150.9, 140.6, 138.6, 136.2, 134.1, 133.4, 128.5, 126.8, 126.4, 124.0, 122.3, 121.3, 120.8, 119.6, 111.4, 109.8, 104.1, 37.1 (N$\underline{C}H_2$), 13.8 ($\underline{C}H_3$).

MS (ESI) *m/z* (%) = 411 (M^+-H, 100).

IR ν_{max} in cm^{-1} (KBr): (C–H Ar) 3046; (C–H Al) 2975; (–C≡N) 2219; (C=C Ar) 1592, 1498; (C–H Ar) 747.

3-(3-Cyanocarbazol-9-yl)-9-ethylcarbazole (2) was prepared according to the procedure similar to that described for the synthesis of **1**. 3-Iodo-9-ethylcarbazole (0.72 g, 2.25 mmol), 3-cyanocarbazole (0.3 g, 1.5 mmol), K_2CO_3 (0.62 g, 4.5 mmol), Cu (0.19 g, 3 mmol), 18-crown-6 (0.04g), and 10 ml

of *o*-DCB were used. The reaction mixture was refluxed under nitrogen atmosphere for 24 h. The product was purified by silica gel column chromatography using hexane/ethylacetate (10/1) as an eluent. The target compound was obtained as yellow crystals (fw = 385 g/mol, mp = 214–216 ^{o}C) in 78% (0.45 g) yield.

^{1}H NMR (400 MHz, $CDCl_3$) δ (ppm): 8.50 (s, 1H, Ar), 8.23 – 8.21 (m, 2H, Ar), 8,11 (d, J = 7.8 Hz, 1H, Ar), 7.67 – 7.64 (m, 2H, Ar), 7.60 – 7.48 (m, 4H, Ar), 7.42 – 7.38 (m, 3H, Ar), 7.31 (t, J = 8.0 Hz, 1H, Ar), 4.52 (q, J = 7.2 Hz, 2H, N$\underline{C}H_2$), 1.57 (t, J = 7.2 Hz, 3H, $\underline{C}H_3$).

^{13}C NMR (100 MHz, $CDCl_3$) δ (ppm): 143.6, 142.8, 140.7, 139.5, 129.1, 127.4, 127.3, 126.7, 125.3, 124.8, 124.0, 123.2, 123.0, 122.4, 122.0, 120.9, 119.6, 119.5, 110.7, 110.6, 109.7, 108.9, 102.2, 37.9 (N$\underline{C}H_2$), 13.9 ($\underline{C}H_3$).

MS (ESI) *m/z* (%) = 386 (M^++H, 30).

IR ν_{max} in cm^{-1} (KBr): (C–H Ar) 3047; (C–H Al) 2972, 2929; (–C≡N) 2214; (C=C Ar) 1595, 1472; (C–H Ar) 807, 747.

2-(3-Cyanocarbazol-9-yl)-9-ethylcarbazole (3). To a dry, three-necked round flask 2-bromo-9-ethylcarbazole (1 g, 3.6 mmol), 3-cyano-9H-carbazole (1.04 g, 5.4 mmol), t-BuOK (2 g, 18 mmol), CuI (1.4 g, 7.2 mmol), 2,2,6,6-tetramethyl-3,5-heptanedione (TMHDO, 0.4 ml), and anhydrous DMF (20 mL) were charged. The mixture was degassed and refluxed under nitrogen atmosphere for 24 h. After cooling to room temperature, the reaction mixture was poured into water, extracted with ethyl acetate, washed with 3 N HCl and water. After being dried over Na_2SO_4 and filtered, the solvent was removed and the crude product was purified by silica gel column chromatography using hexane/tetrahydrofuran (9/1) as an eluent. The product was crystallized from methanol and was obtained as yellowish crystals (fw = 385 g/mol, mp = 187–188 ^{o}C) in 47% (0.65 g) yield.

^{1}H NMR (700 MHz, $CDCl_3$) δ (ppm): 8.39 (s, 1H, Ar), 8.21 (d, J = 8.0 Hz, 1H, Ar), 8.10 (d, J = 7.8 Hz, 2H, Ar), 7.56 (dd, J=8.5, 1.5 Hz, 1H, Ar), 7.48 – 7.37 (m, 6H, Ar), 7.30 (t, J = 7.4 Hz, 1H, Ar), 7.24 (m, 2H, Ar), 4.29 (q, J=7.2 Hz, 2H, $NC\underline{H}_2$), 1.36 (t, J = 7.2 Hz, 3H, $C\underline{H}_3$).

^{13}C NMR (176 MHz, $CDCl_3$) δ (ppm): 142.1, 141.2, 139.7, 139.5, 132.8, 128.2, 126.4, 125.4, 124.3, 122.4, 122.0, 121.4, 121.1, 120.7, 120.1, 119.7, 119.6, 119.5, 118.6, 116.8, 109.7, 109.5, 107.8, 106.2, 101.5, 36.8 ($N\underline{C}H_2$), 12.8 ($\underline{C}H_3$).

MS (ESI) m/z (%) = 386 (M^++H, 100).

IR ν_{max} in cm^{-1} (KBr): (C–H Ar) 3060; (C–H Al) 2972, 2932; (–C≡N) 2220; (C=C Ar) 1597; (C–H Ar) 810, 739.

3-(2,7-Dicyanocarbazol-9-yl)-9-ethylcarbazole (4) was prepared according to the procedure similar to that described for the synthesis of **1**. 3-Iodo-9-ethylcarbazole (2.2 g, 6.9 mmol), 2,7-dicyanocarbazole (1.5 g, 6.9 mmol), K_2CO_3 (7.62 g, 55.2 mmol), Cu (1.75 g, 27.6 mmol), 18-crown-6 (0.73g), and 30 ml of *o*-DCB were used. Reaction mixture was refluxed under nitrogen atmosphere for 72 h. The product was purified by silica gel column chromatography using hexane/tetrahydrofuran (9/1) as an eluent. The target compound was obtained as greenish crystals (fw = 410 g/mol, mp = 270–272 ºC) in 20% (0.55 g) yield.

^{1}H NMR (700 MHz, $CDCl_3$) δ (ppm): 8.17 (d, J = 8.0 Hz, 2H, Ar), 8.08 (s, 1H, Ar), 8.00 (d, J = 7.8 Hz, 1H, Ar), 7.60 (s, 2H, Ar), 7.56 (d, J = 8.1 Hz, 1H, Ar), 7.50 – 7.46 (m, 3H, Ar), 7.45 – 7.40 (m, 2H, Ar), 7.20 (t, J = 7.5 Hz, 2H, Ar), 4.41 (q, J = 7.5 Hz, 1H, $NC\underline{H}_2$), 1.46 (t, J = 7.3 Hz, 3H, $C\underline{H}_3$).

^{13}C NMR (176 MHz, $CDCl_3$) δ (ppm): 141.1, 139.7, 138.7, 125.9, 125.1, 124.0, 123.4, 123.2, 122.4, 121.1, 120.9, 119.8, 118.7, 118.4, 113.9, 109.4, 109.0, 108.0, 36.9 ($N\underline{C}H_2$), 12.9 ($\underline{C}H_3$).

MS (ESI) m/z (%) = 411 (M^++H, 35).

IR ν_{max} in cm^{-1} (KBr): (C–H Ar) 3053; (C–H Al) 2978, 2924; (–C≡N) 2227; (C=C Ar) 1496; (C–H Ar) 806.

3. Results and Discussion

3.1. Synthesis

Compounds **1**–**4** were synthesised as shown in Scheme 1 by Ullmann C-N coupling reaction. The chemical structures of the synthesized compounds were confirmed by ^{1}H and ^{13}C NMR, IR spectroscopies, and mass spectrometry.

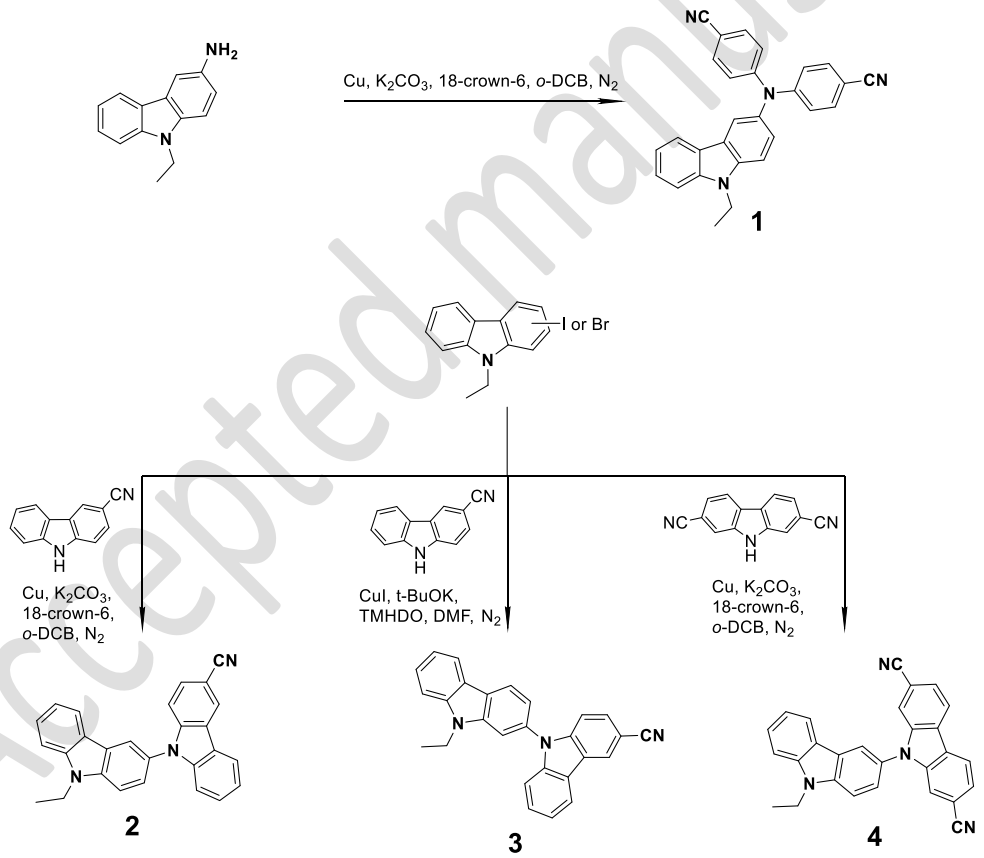

Scheme 1. Synthesis of compounds **1**–**4**.

3.2. Thermal properties

The behavior under heating of the synthesized compounds was studied by DSC and TGA under nitrogen amosphere. The values of the glass transition temperatures (T_g), melting points (T_m), and temperatures at which 5% loss of mass was observed (T_{ID}) are summarized in Table 1. All the synthesized compounds demonstrated high thermal stability. The values of T_{ID} were found to be higher than 300 °C, as confirmed by TGA with a heating rate of 10 °C/min. The highest T_{ID} was observed for dicyanocarbazolyl substituted compound **4** (359 °C).

All the synthesized compounds (**1**–**4**) were obtained as crystalline substances. However, they readily formed glasses when their melt samples were cooled down. For the illustration of above stated the DSC curves of compound **2** are shown in Fig. 1. In the first DSC heating scan, compound **2** showed endothermic melting signal at 224 °C. The compound formed glass upon cooling from the melt. In the following heating scan, compound **2** showed glass transitions at 79 °C.

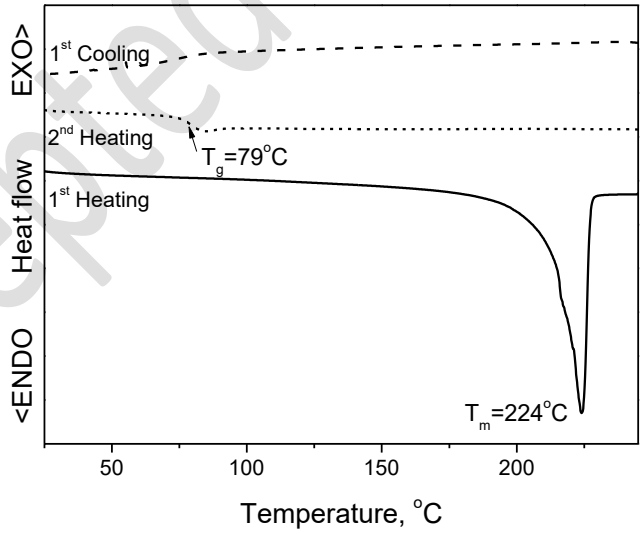

Figure 1. DSC curves of **2** (scan rate 10 °C/min, N_2 atmosphere).

The glass transition temperatures of the synthesized carbazole compounds depended upon the nature and positions of the substituents. Dicyanodiphenylamino-substituted derivative **1** exhibited lower T_g

than dicyanocarbazolyl substituted compound **4**, apparently, due to the higher flexibility of diphenylamino moiety. Compound **3** having 3-cyanocarbazolyl group at C-2 position of 9-ethylcarbazole moiety ehibited higher T_g by 14 ^{o}C than its isomer (**2**) having the same substituent at C-3 position of 9-ethylcarbaole moiety.

Table 1. Thermal characteristics of compounds **1**–**4**.

Compounds	T_m,[a] ^{o}C	T_g,[a] ^{o}C	T_{ID},[b] ^{o}C
1	176	77	333
2	224	79	302
3	191	93	320
4	261	111	359

[a] Determined by DSC, scan rate 10 ^{o}C/min, N_2 atmosphere.
[b] 5 % weight loss determined by TGA, heating rate 10 ^{o}C/min, N_2 atmosphere.

3.3. Theoretical calculations

The structures of compounds **1–4** were optimizated and the values of the highest occupied molecular orbital (HOMO) and the lowest unoccupied molecular orbital (LUMO) energies were estimated by the density functional theory (DFT) with the B3LYP energy functional and the 6-31G(d,p) basis set in vacuum. The calculations were done using Spartan'14 programme [39]. The theoretical structures and HOMO – LUMO values of compounds 1–4 are given in Figure 2.

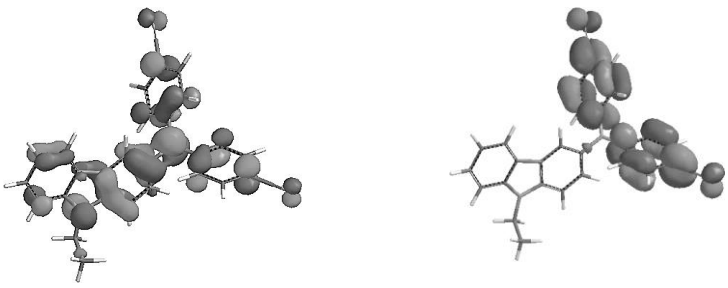

1 HOMO = -5.50 eV LUMO = -1.65 eV

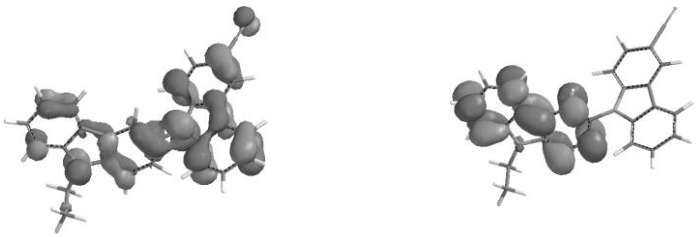

2 HOMO = -5.56 eV LUMO = -1.19 eV

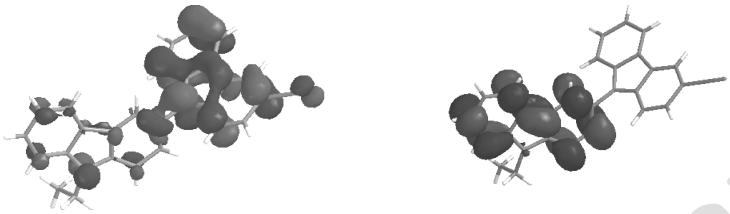

2a HOMO = -5.60eV LUMO = -1.11 eV

3 HOMO = -5.66 eV LUMO = -1.24 eV

4 HOMO = -5.80 eV LUMO = -2.05 eV

Figure 2. Theoretical structures and HOMO – LUMO values of compounds **1**–**4**.

The DFT calculations revealed that HOMO are distributed mostly over the both carbazole moieties for **2**–**4** and over the carbazole and cyano substituted diphenylamino moiety for **1**. The theoretical HOMO values range from -5.80 to -5.50 eV. These values are in good agreement with the experimental data (Table 5). The dihedral angles between the carbazole chromophores of compounds **2**–**4** were calculated to be 54–58^{o}. These dihedral angles are insufficient for the spatial separation of the HOMO and LUMO orbitals on the donor and acceptor moieties. The similar theoretic results were earlier reported for 9-ethyl-9*H*-3,9'-bicarbazole [40], LUMO of compounds **1**

and **4** having two cyano groups were found to be localized on the cyano substituted carbazole or diphenylamino moieties. However, for compounds **2** and **3** with one cyano group the LUMO is localized on the N-ethyl substituted carbazole moiety.

3.4. Photophysical properties

UV-vis spectra of 10^{-4} M solutions of compounds **1**–**4** in THF are shown in Figure 3A while those of the thin films are depicted in Figure 3B. The optical characteristics are summarized in Table 2. The absorption spectra of the solid films of the synthesized compounds **1**–**4** showed small red shifts of 5–12 nm with respect of those of dilute THF solutions. Using the edge wavelengths of the absorption bands, the optical band gaps (E_g^{opt}) were estimated for the synthesized compounds **1**–**4**. The optical band gaps of the solid samples of the synthesized compounds except **3** were found to be shorter than those of the dilute solutions, apparently, due to the enhanced intermolecular interactions.

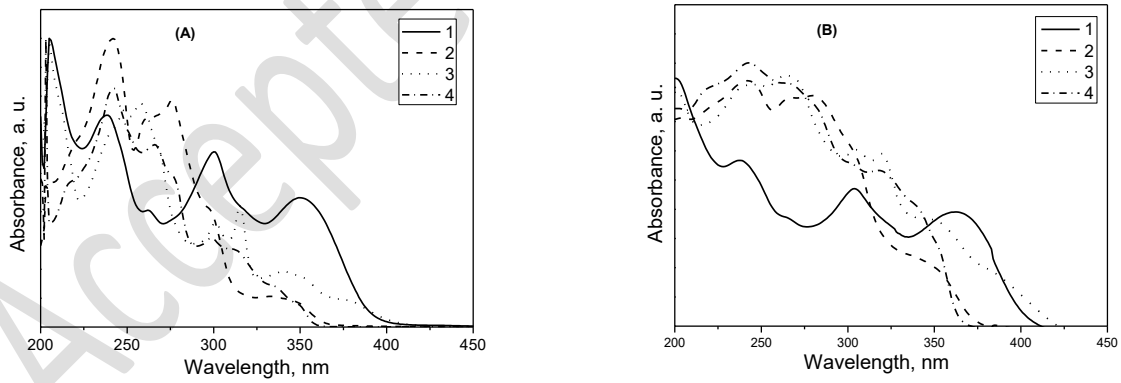

Figure 3. UV-vis absorbtion spectra of the dilute solutions (A) and of neat films (B) of the synthesized compounds **1**–**4**.

PL quantum yields were estimated for the dilute solutions and for the neat films of the compounds. The data are summarized in Table 2 The highest PL quantum yields were observed for the solution and the neat film of compound **4**. Cyanocarbazolyl-substituted carbazoles **2**–**4** showed considerable decrease of PL quantum yields in the solid state as compared to those of the solutions. In contrast, PL quantum yield of the solid sample of dicyanophenylamino substituted carbazole **1** was found to be comparable with that of the dilute solution. As dicyanophenylamino substituted compound **1** has more freedome for the rotation of N-C bonds compared with cyanocarbazolyl-substituted compounds **2-4**, such PL quantum yield of **1** in the solid state can aperently be explained by aggregation-induced emission enhancemenn [41].

Table 2. Photophysical properties of 10^{-5} M THF solutions and thin films of **1**–**4**.

Compound	Dilute solution				Thin film			
	UV: λ_{edge}, nm	E_g^{opt}, eV	$\lambda_{max,PL}$, nm	Φ_{PL}, %	UV: λ_{edge}, nm	E_g^{opt}, eV	$\lambda_{max,PL}$, nm	Φ_{PL}, %
1	392	3.16	480	14.80	404	3.07	457	14.28
2	364	3.40	385	24.46	374	3.32	392	5.20
3	404	3.07	374	32.65	415	2.99	378, 494*	<1
4	357	3.47	480	49.87	362	3.43	475	26.41

*shoulder

To study possibility of the TADF effect for the synthesized compounds, the phosphorescence spectra of the THF solutions of **1-4** were recodered (Figure 4A). The phosphorescence was excited by UV radiation of 300 nm for all the samples. The singlet (S_1), triplet (T_1) energies and singlet–triplet energy splittings (ΔE_{ST}) observed for compounds **1–4** are summarized in Table 3. The values

of S_1 and T_1 of **1–4** were determined from the onsets of the fluorescence and phosphorescence spectra, respectively. It is possible to predict that compounds **1–4** can be utilized as functional materials for efficient visible color OLEDs due to the high values of T_1 (2.76–3.02 eV). TADF can be predicted for compound **4** because of the low ΔE_{ST} value (0.16 eV). To prove this assumption we additionally recorded PL spectrum of the solution compound **4** after elimination of oxygen. The intensity of PL of the degassed THF solution of **4** was found to be by ca. two times higher than that of the non-degassed THF solution (Figure 4B). The PL decay curves of both degassed and non-degassed THF solutions of **4** showed the monoexponential character (Figure 4C). The PL life time of 21.7 ns of degassed THF solution was found to be longer than that of the non-degassed solution (12.9 ns). Despite of the increase of the PL intensity and PL life time of the solution of **4** after purging it with the inert gass, TADF component was not observed in the PL decay curve (Figure 4C, insert). It is usually are observed in the μs range or even ms range and it has double exponential character including prompt and delay fluorescence [42]. The increase of the PL intensity and PL life time of **4** upon elimination of oxygen was apparently observed due to the triplet-triplet annihilation that is caused by the intersystem [43].

Table 3. Singlet and triplet energies of compounds **1-4**[1]

	1	**2**	**3**	**4**
Singlet state energy (S_1), eV	3.26	3.41	3.49	2.92
Triplet state energy (T_1), eV	2.79	3.02	2.93	2.76
Singlet–triplet energy splitting (ΔE_{ST}), eV	0.47	0.39	0.56	0.16

[1] Estimated for 10^{-5} M THF solutions

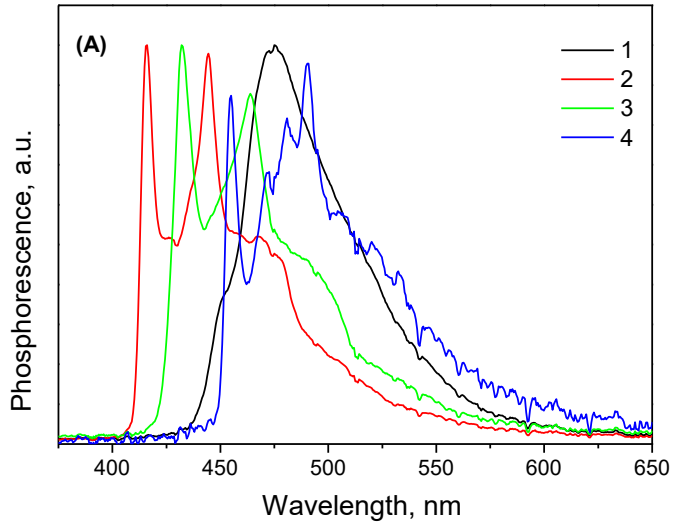

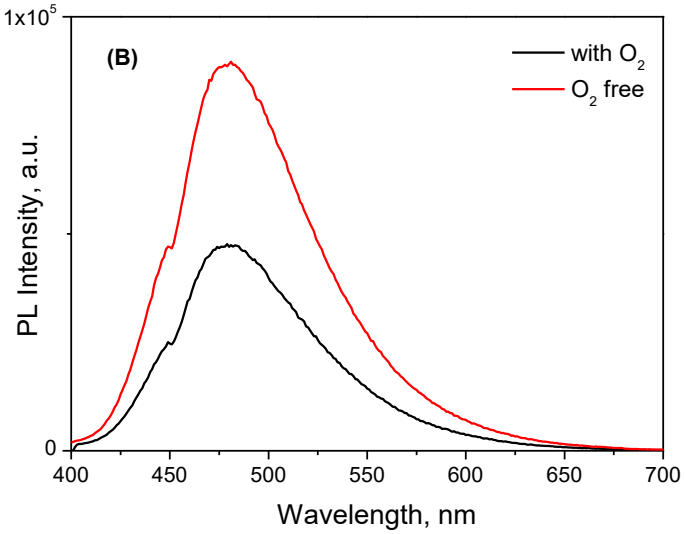

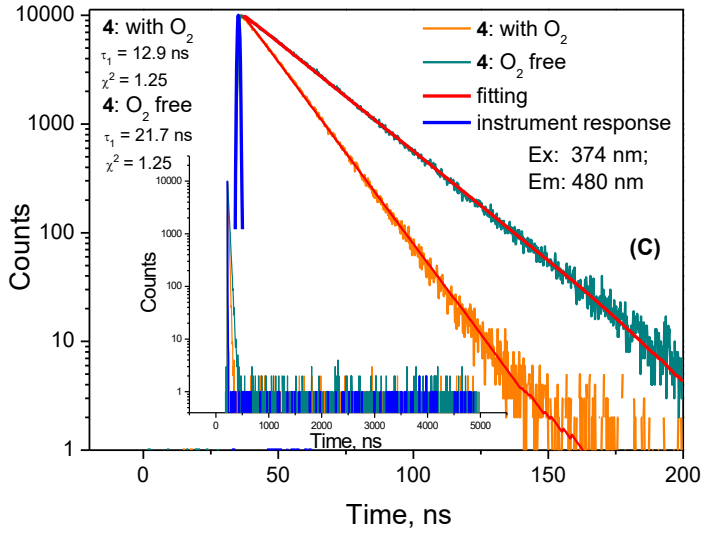

Figure 4. Phosphorescence spectra of the solutions of compounds **1**–**4** in THF (10^{-5} M) recorded at 77 K (A); photoluminescence spectra of **4** in degassed and non-degassed THF solutions (B); and normalized photoluminescence decay curves of the solution of **4** in THF before and after degassing (C).

The colour coordinates were calculated from PL spectra of neat films according to CIE recommendations [44]. The emission of the film of **2** was in the range of blue colour while derivatives **1, 3** and **4** showed blue sky emission (Table 4).

Table 4. CIE colour coordinates of PL of the films of **1–4.**

Derivative	X	Y
1	0.218	0.342
2	0.188	0.163
3	0.205	0.263
4	0.181	0.306

3.5. Eelectrochemical properties and ionization potentials

Electrochemical properties of the solutions of the synthesized compounds **1–4** in dichloromethane with 0.1 M tetrabulthylammonium hexafluorophosphate as supporting electrolyte were studied by the cyclic voltammetry (CV) using $Ag/AgNO_3$ as the reference electrode and a Pt wire counter electrode. Taking 4.8 eV as the ionization potential (IP_{CV}) value for the ferrocene redox system related to the vacuum level, the IP_{CV} and electron affinity (EA_{CV}) values of compounds **1–4** were estimated. The electrochemical characteristics are summarized in Table 5.

The CV curves of compounds **2** and **4** are shown in Figure 5 All the synthesized compounds showed the oxidation waves up to ca 2 V. The oxidation was found to be reversible only for dicyanodiphenylamino substituted carbazole derivative **1**. The cyanocarbazolyl substituted carbazole compounds **2–4**, having unsubstituted reactive C-6 or C-3 and C-6positions of carbazole rings showed irreversible oxidation. Irreversible oxidation of **2–4** was followed by coupling of carbazole radical cations because of the higher electron spin density at C-3 and C-6 positions [45] and formation of new carbazole-containing componds [46]. No reduction potentials were recorded for the samples of compounds **2** and **3** containing single cyano groups, while compounds **1** and **4** having two cyano groups showed reduction potentials ranging from -2.07 V to -1.97 V.

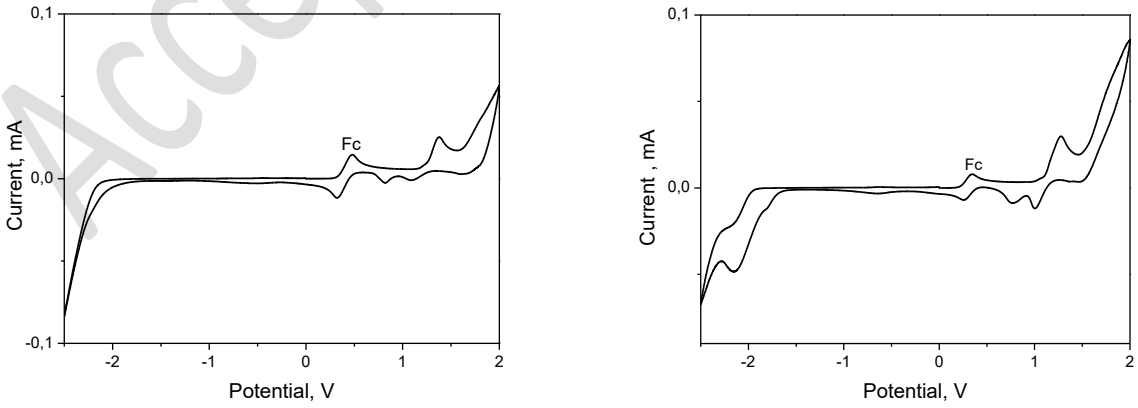

Figure 5. Cyclic voltammograms of argon-purged dichloromethane solutions of **2** and **4** (scan rate 50 mV/s).

An important characteristic of electronically active compounds intended for the application in optoelectronic devices is ionization potential (IP), which characterizes the electron releasing work under illumination. The IP_{CV} values deduced from the onset redox potentials ranged in a small window (5.34–5.69 eV). The values of the ionization potentials (IP_{EP}) of the solid samples of compounds **1–4** were estimated by electron photoemission spectrometry. The spectra are shown in Figure 6 and the results are collected in Table 5.

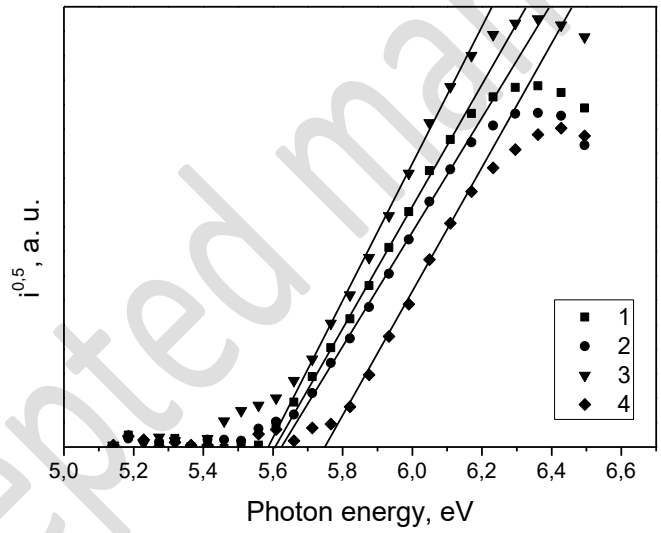

Figure 6. Photoelectron emission spectra of the layers of **1–4**.

The IP_{EP} of the layers of compounds **1–4** range from 5.58 to 5.75 eV, indicating good air stability for these materials. While the range IP_{CV} values are generally a little smaller than those estimated by the photoemission spectrometry, both methods provide the same trend.

Table 5. Electrochemical characteristics of derivatives **1–4**.

	E_{red}^{onset},[a] V	E_{ox}^{onset},[a] V	IP_{CV},[b] eV	EA_{CV},[b] eV	E_g^{elc},[c] eV	E_g^{opt},[d] eV	IP_{EP},[e] eV
1	-2.07	0.54	5.34	-2.73	2.61	2.98	5.60
2	Not fixed	0.84	5.64	-	-	2.84	5.63
3	Not fixed	0.89	5.69	-	-	3.22	5.75
4	-1.97	0.77	5.57	-2.83	2.74	3.38	5.58

[a] E_{red}^{onset} and E_{ox}^{onset} are measured vs. ferrocene/ferrocenium. [b] Ionization potentials and electron affinities estimated according to $IP_{CV} = (E_{ox}^{onset} + 4.8)$. $EA_{CV} = (E_{red}^{onset} + 4.8)$ (where, E_{ox}^{onset} and E_{red}^{onset} are the onset reduction and oxidation potentials versus the Fc/Fc^+). [c] $E_g^{elc} = IP_{CV} - EA_{CV}$, where E_g^{elc} is the electrochemical band gap. [d] The optical band gap of the solid samples of the compounds estimated from the onset wavelength of optical absorption spectra according to the formula: $E_g^{opt} = 1240/\lambda_{edge}$, in which the λ_{edge} is the onset value of absorption spectrum in long wave direction. [e] Established from photoelectron emission spectra.

3.6. Charge-transporting properties

Charge-transporting properties of the synthesized compounds **1–4** were studied by the time of flight (TOF) method. The TOF transients for holes of a thin layer of **1** are shown in Figure 7A. The dispersive hole transport was observed for the layer of compound **1**. The transit times practically were not observed in the linear plots; however, they were well seen on log-log plots. Much more dispersive hole transport was found for compound **2** and **4**. As an example, the TOF transients for a thin layer of **4** were ploted in Figure 7B. The similar transients were observed for the layer of the compound **2**. The transit times for holes of compound **3** were not found due to the strong dispersity. Despite of the bipolar (donor-acceptor) nature of compounds **1–4** the transit times for electrons were not recognized.

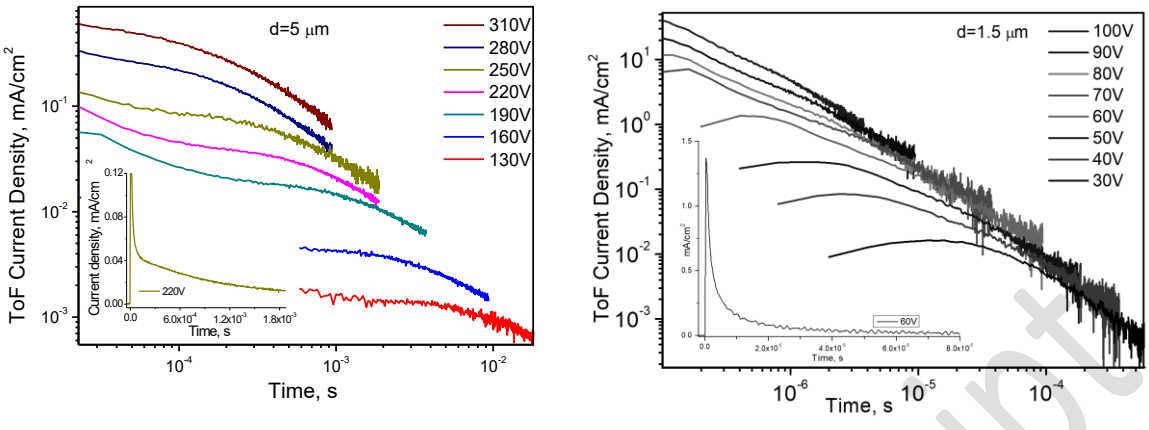

(A) (B)

Figure 7. Time of flight transients for holes in thin layers of compounds **1** (A) and **4** (B). The insets show transient curves in the linear plots.

The dependencies of the hole drift mobilities on the square root of electric field for compounds **1**, **2** and **4** are shown in Figure 8. The obtained hole mobility (μ) value for dicyanocarbazolyl substituted carbazole compound **4** was found to be 2 orders of magnitude higher than that for dicyanodiphenylamino substituted carbazole derivative **1**. The value of μ of **4** was found to be 2.33×10^{-4} cm^2/Vs, whereas μ of 7.67×10^{-6} cm^2/Vs was observed for compound **1** at electrif field of 6.4×10^5 V/cm. Hole mobilities of the layer of compound **2** were found to be only slightly lower than those of the layer of compound **4**. This observation shows that the number of cyano groups practically does not affect hole mobility. The inferior hole-transporting properties of dicyanodiphenylamino substituted carbazole derivative **1** compared to those of dicyanocarbazolyl substituted carbazole compounds **2** and **4** can apparently be explained by the volume effects in the solid state layer due to the enhanced non-planarity of the molecules of **1** relative to those of **2** and **4**. Hole mobility of **1** is lower than that of many other carbazole derivatives [47, 48, 49]. The

molecules of **1** are apparently completely disordered in the solid state layer because of the non-planar molecular structure.

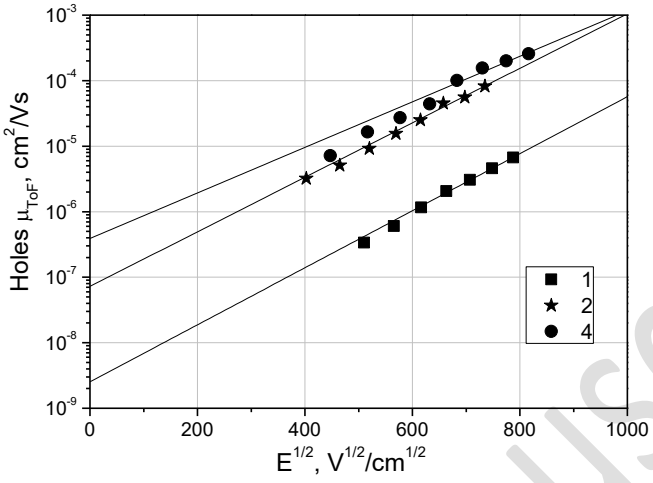

Figure 8. Hole drift mobilities as a function of $E^{1/2}$ for the layers of **1**, **2** and **4**.

3.7.Device fabrication and characterization

The relatively high PL quantum yield, suitable hole mobility and energy levels of compound **4** showed that this compound could be promissing as an emitter for the application in OLEDs. The devices were fabricated by step-by-step deposition or co-deposition of the different layers. MoO_3 or 4,4′,4″-tris[3-methylphenyl(phenyl)amino]triphenylamine (m-MTDATA) were used for the preparation of hole-(injecting) transporting layer [50]. Tris(4-carbazoyl-9-ylphenyl)amine (TCTA) was utilized as the host, and 4,7-diphenyl-1,10-phenanthroline (Bphen) was used for the deposition of electron-transporting layer. The layer of indium tin oxide (ITO) was used as anode, and that of Ca:Al was used as cathode. The structures of devices **A** and **B** were as follows: **A**: ITO/MoO_3/**4**/Bphen/Ca:Al; **B**: ITO/m-MTDATA/TCTA:**4**/Bphen/Ca:Al.

Electroluminescence (EL) spectra of the devices **A** and **B** are depicted in Figure 9A. The device **A** exhibited blue EL. The EL spectrum was very similar to PL spectrum of the solid film of **4**. The

device **A** showed rather low efficiency. The reason of low efficiency of device **A** was poor hole injection in the emission layer. Therefore, the hole-transporting layer of m-MTDATA and TCTA as the host of emitting layer were introduced into the structure of device **B** (Figure 10). Surprisingly, this device exhibited yellow luminescence (Figure 9A). To explain the experimental results, PL spectra of the layers of the molecular mixtures TCTA:**4** and m-MTDATA:**4** were recorded. Although the PL spectra of solid films of the pure materials **4**, TCTA, and m-MTDATA appear in blue region, the molecular mixtures TCTA:**4** and m-MTDATA:**4** exhibited sky blue and orange PL respectively (Figure 9A). This observation can be explained by the formation of exciplexes of the derivative **4** with TCTA and m-MTDATA. Different emission colours of exciplexes TCTA:**4** and m-MTDATA:**4** can be explained utilazing equation $hv_{ex}^{max} \simeq I_P^D - E_A^A - E_C$ for exciplex emission maximum, where I_P^D is the ionization potential of the donor, E_A^A is the electron affinity of the acceptor, and E_C is the electron–hole Coulombic attraction energy (0.35 eV is a typical value for the e-h binding energy in organic materials) [15]. Indeed, the values of $hv_{ex}^{max}(\text{TCTA: } \mathbf{4}) \simeq 2.49$ eV and $hv_{ex}^{max}(\text{m} - \text{MTDATA: } \mathbf{4}) \simeq 1.89$ eV are in good agreement with the emission maxima at 490 nm (2.53 eV) and 584 nm (2.12 eV) of the molecular mixtures TCTA:**4** and m-MTDATA:**4**. The differences between the calculated and measured values could be due the bending of HOMO, LUMO levels at the donor-acceptor interface [51] and to the lack of exact e-h binding energies. As it was expected for exciplex emission, PL decay transients for the molecular mixtures TCTA:**4** and m-MTDATA:**4** were observed in the range up to microseconds (Figure 9B). Such PL decay transients can not be atributed to the emission of **4** which was observed in the ns range (Figure 4C). The PL decay curves of the the solid layers of the mixtures TCTA:**4** and m-MTDATA:**4** could be adequately described (χ^2=1.173 and 1.289, respectively) by the double exponential law A+B1exp(-t/τ_1)+B2exp(-t/τ_2). The PL lifetimes of 45 ns and 56 ns respectively are apparently related to exciplex emission, while the lifetimes of 193 ns and 305 ns can be explaned by TADF effect of

exciplexes due to the reverse intersystem crossing (RISC) from singlet to triplet state [52, 53]. RISC can occur due to the small singlet-triplet energy splitting (ΔE_{ST}) of exciplex, wich was found to be of 0.05 eV for TCTA:**4**. Figure 9C depicts PL spectra of the molecular mixture TCTA:**4** at the different temperatures. The curves were recorded without delays imediately after excitation. PL decay curves of the layer of the molecular mixture TCTA:**4** recorded at the different temperatures are shown in the insert of Figure 9C. They show two decay components displaying that PL spectra of the TCTA:4 exciplex included the weak prompt fluorescence and strong phosphorescence at low temperatures while at room temperature the PL spectra consisted of prompt and delay fluorescence. The presence of two decay components with the similar character was previously observed for the exciplexes exhibitting TADF effect [52, 54].To prove the asumption that the long-lived components of the PL decay curves of the layers of the mixtures TCTA:**4** and MTDATA:**4** appeared due to the TADF effect of the exciplexes, PL intensity dependences of the molecular mixtures TCTA:**4** and m-MTDATA:**4** on the laser flux were recorded (Figure 9D). The linear dependence with slope of ca. 1 of PL intensity on laser flux was observed for the studied mixtures TCTA:**4** and MTDATA:**4**. This observation shows that exciplex TADF effect is responsible for the long-lived PL components of the molecular mixtures [55].

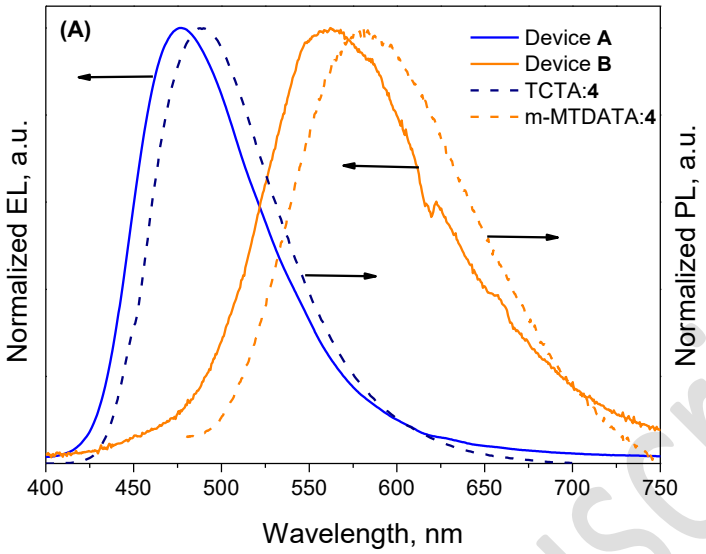

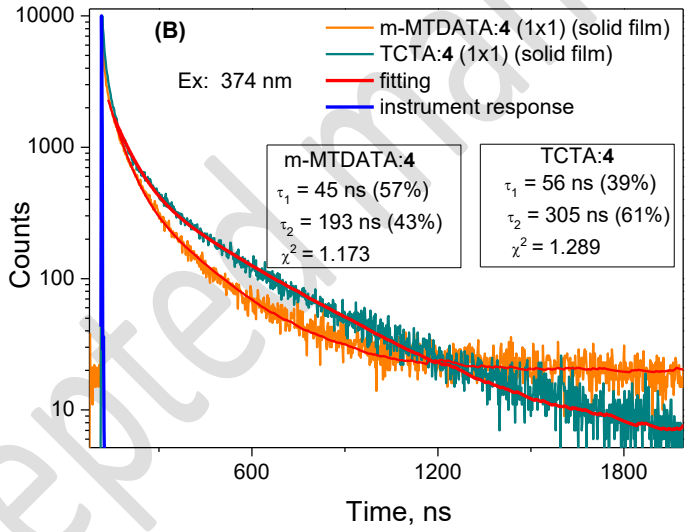

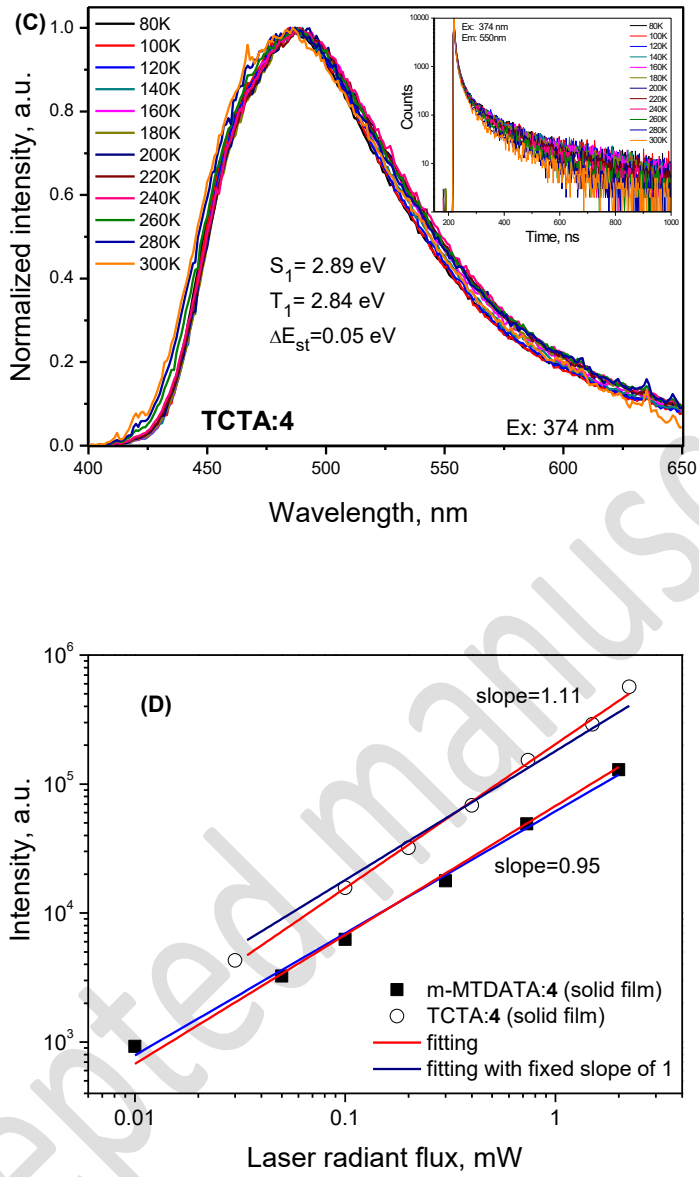

Figure 9. (A) EL spectra of devices **A** and **B** recorded at 10V and PL spectra of the layers of the mixtures TCTA**:4** and m-MTDATA**:4;** (B) normalized photoluminescence decay curves of the solid films of the molecular mixtures; (C) PL spectra and PL decay curves (insert) of the layer of the molecular mixture TCTA:**4,** and (D) TCTA:**4** and MTDATA:**4** PL intensity dependencies on laser flux.

The EL spectrum of the device **B** shown in Figure 9A does not coincided with the PL spectra of the layers of the mixtures TCTA:**4** and m-MTDATA:**4**. The possible explanation of this observation could be that the EL spectrum of the device **B** was a obination of exciplex emissions of both TCTA:**4** and m-MTDATA:**4** (Figure 10). The exciplex emission of TCTA:**4** (PLQY = 43.8 %) was more efficient than the exciplex emission of m-MTDATA:**4** (PLQY = 3.84 %). However, the energy of EL of the device **B** is close to that of the exciplex PL of m-MTDATA:**4** (Figure 9A). This observation can apparently be explained by the energy transfer from the exciplex TCTA:**4** to the exciplex m-MTDATA:**4** (Figure 10).

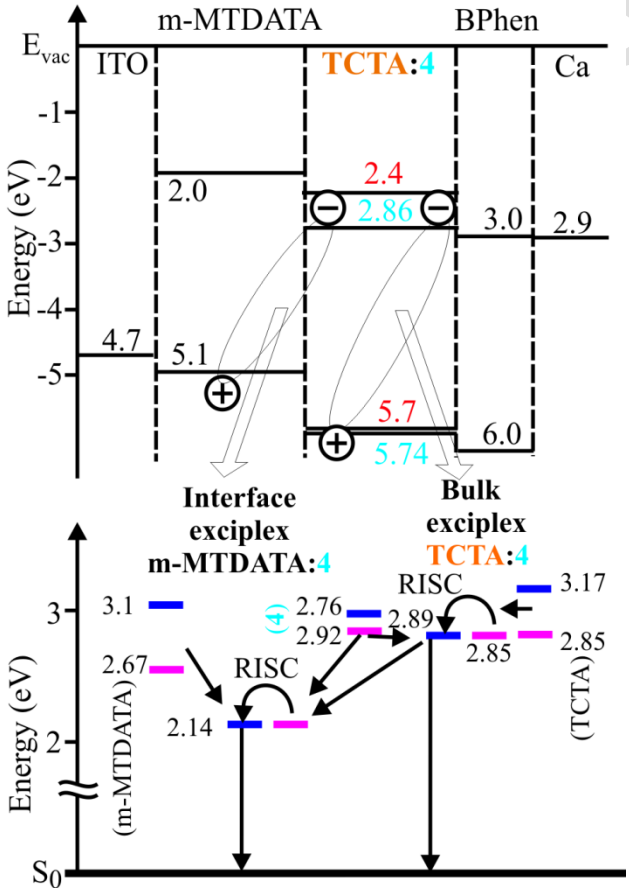

Figure 10. The energy diagram of the device **B**, and locations of interface m-MTDATA:**4** and bulk TCTA:**4** exciplexes (top). Singlet and triplet energy levels of m-MTDATA, **4**, TCTA, and the

resultant exciplexes m-MTDATA:**4** and TCTA:**4** (bottom). Singlet and triplet energy levels are marked by blue and pink colors, respectively.

To support our assumption on the energy transfer from the bulk exciplex TCTA:4 to the interface exciplex m-MTDATA:4 in device B, we carried out the additional experiments regarding the fabrication and characterization of exsiplex-based OLEDs formed only with m-MTDATA:4 and TCTA:4 as emitters. We have fabricated new OLEDs (devices C and D) the structures of which were as follows: ITO/m-MTDATA/TCTA/TCTA:**4**/**4**/Bphen/Ca:Al (device C) and ITO/m-MTDATA/m-MTDATA:**4**/**4**/Bphen/Ca:Al. To avoid formation of exciplexes except for the needed one, non-doped layers of TCTA and/or **4** were included into the structures of the devices C and D.

Figure 11 shows that the EL spectra of these devices recorded at the different applied voltages are similar to the PL spectra of the molecular mixtures TCTA:4 and m-MTDATA:4 which exhibited sky blue and orange PL respectively (Figure 9A and 11). The maximum intensity of EL spectrum for device C (at ca. 490 nm) was observed at the same wavelength as that of PL spectrum of the molecular mixture TCTA:4 (Figure 11). The maximum of EL spectrum observed for device D at ca. 598 nm was shifted to the low energy region by 14 nm compared to that of the PL spectrum of the molecular mixture m-MTDATA:4 apparently due to the different excitations involved (optical/electrical). Such blue shift of EL spectrum compared to the solid-state PL spectrum of the exciplex emitter was earlier reported and was explained by the enhancement of the delayed fluorescence by the electrical excitation of the exciplex emission [56]. In contrast, the intensity maximum of EL spectrum for device B observed at ca. 560 nm was shifted to the high energy region by 38 nm compared to that of device D. This observation shows that the mechanism of EL of device B (Figure 11) is different. Most probably, it is the energy transfer from the bulk exciplex TCTA:4 to

the interface exciplex m-MTDATA:4 in the device B since the shapes of EL spectra of both devices B and D on the m-MTDATA:4 exciplex are also very similar. In addition, lower maximum external quantum efficiencies of 4.2 and 3.2 % observed for devices C and D were lower than that of device B (5.8%) (Table 6). This result also indicates that energy transfer occurs in device B leading to the change of EL colour and to the enhancement of external quantum efficiency. The output characteristics of sky-blue and orange exciplex-based OLEDs are additionally presented in Figures 12 and 13 and included in Table 6.

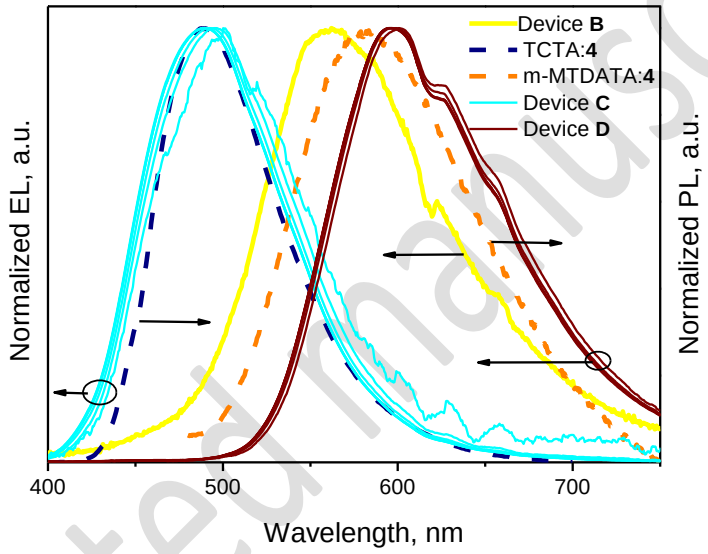

Figure 11. PL spectrum of the solid film of the molecular mixtures TCTA:4 and m-MTDATA:4 *vs.* EL spectra of device B as well as of devices C, and D (recorded at applied voltages from 4 to 10 V).

As shown in Figure 12, devices **A** and **B** exhibited low turn-on voltages (V_{on}) of 3.5 and 4.5 V, respectively. The low turn-on voltages could be ascribed to the effective hole injection due to suitable HOMO energy level of the derivative **4**. Figure 12 also shows current density–voltage–luminance curves of the devices **A** and **B**. The maximum luminance of device **A** did not reach 3000 cd/m^2 while that of the device **B** was over 6000 cd/m^2. The brightness of device **B** was also much

higher than that of the device **A**. This observation can apparently be explained by the higher hole mobility of TCTA relative to that of derivative **4**. One more reason of the poor performance of device **A** might be unbalanced hole and electron mobilities in the emitting layer of **4**. The balanced hole and electron mobilities are of extreme importance for the materials of emitting layers [57].

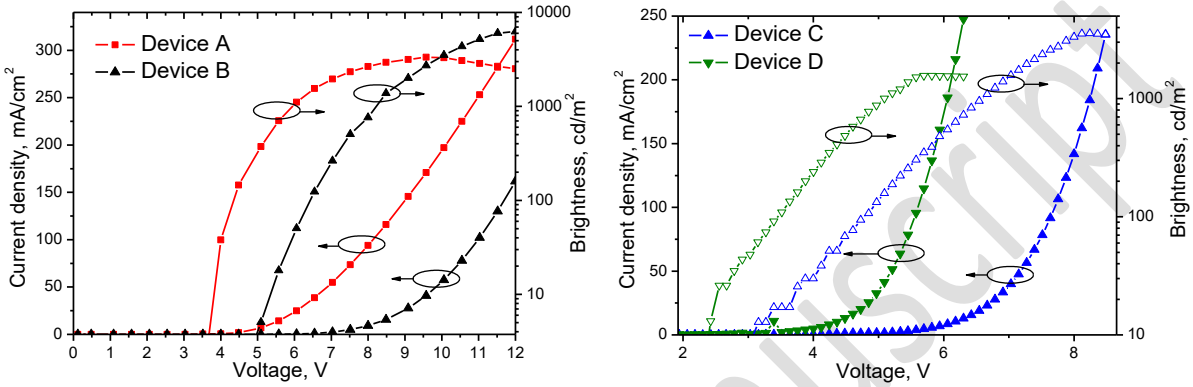

Figure 12. Current density-voltage-brightness characteristics of the studied devices.

External quantum efficiency (EQE)–current density curves for OLEDs **A** and **B** are shown in Figure 13. The characteristics of the devices are summarized in Table 6. The device **B** exhibited much higher maximum EQE than the device **A** at the same luminance. The maximum quantum efficiencies of 2.0 and 5.8% were observed for devices **A** and **B**, respectively. The CIE color coordinates were calculated to be (0.17, 0.28) and (0.40, 0.52) for devices **A** and **B**, respectively. We note that triplet energy levels of **4**, TCTA, and m-MTDATA, which could be sources of energy losses in the emitting layer, are higher than exciplex energy levels denying the possibility of energy losses through the triplets (Figure 13). The external quantum efficiencies observed at 1000 cd/m2 were used to calculate the efficiency roll-offs which were in the range from 28 to 61 % for the studied devices (Table 6). It should be pointed out that the characteristics of OLEDs were recorded for the devices under ordinary laboratory conditions. Using variety existing materials [58, 59], the

device performance could be further improved by changing the hole and electron transporting layers, optimizing the layer thicknesses, changing concentration of **4** in the host, varying the processing conditions.

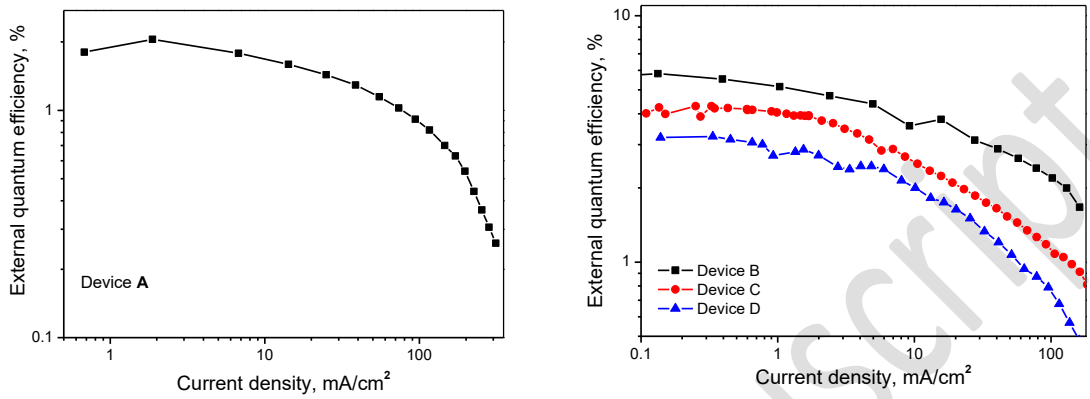

Figure 13. External quantum efficiency-current density characterictic of the studied devices.

Table 6. EL characteristics of the studied devices.

Devices	Von (V)	Max. brightness (cd/m2)	Max. current efficiency (cd/A)	Max. power efficiency (lm/W)	Max. external quantum efficiency (%)	Rol-off efficiency (%)[a]
A	3.5	2515	7.7	5.4	2.0	28
B	4.5	6260	13.48	8.1	5.8	38
C	3.2	3600	9.9	8.8	4.2	52
D	2.5	1570	5.5	5.3	3.2	61

[a] calculated at brightness of 1000 cd/m^2

Conclusions

A series of carbazole based compounds containing cyano groups were synthesized and characterized. The thermal, photophysical, electrochemical, charge-transporting properties of the synthesized compounds were studied. The compounds exhibited relatively high thermal stability with 5 % weight loss temparatures ranging from 302 to 359 ^{o}C. They were capable of glass formation with the glass transition temperatures of 77–111 ^{o}C. Ionization potentials of the layers of

the compounds established by electron photoemission spectrometry were found to in the shoert range of 5.58–5.75 eV. Time-of-flight hole mobilieties of the layers of carbazolyl-substituted carbazoles with cyano groups were found to be considerably higher than those of dicyanophenylamino-substituted derivative and exceeded 10^{-4} cm^2/Vs at high electric fields. 3-(2,7-Dicyanocarbazol-9-yl)-9-ethylcarbazole was used as emitter for the fabrication undoped and doped electroluminescent devices. Exciplex TADF was identified for the mixtures of the cyano-substituted carbazole derivative and commercial donor materials. This finding allowed us to develop a new approach for the fabrication of effective OLEDs in wich both interface and bulk exciplexes were utilized as emitters. The undoped device showed blue electroluminescence with the maximum external quantum efficiency of 2.0 %. The doped device showed yellow exciplex TADF emission with the maximum external quantum efficiency of 5.8 %. Sky-blue and orange OLEDs containing one exciplex-based emitter were additionaly fabricated and showed external quantum efficiencies of 4.2 and 3.2 %, respectively.

Acknowledgement

This research was supported by H2020-ICT-2014/H2020-ICT-2014-1 project PHEBE (grant agreement No 641725).

References

[1] Reineke. S. Complementary LED Technologies. Nature Mater. 2015;14:459−462.

[2] Fyfe. D. LED Technology. Organic Displays Come of Age. Nat. Photonics 2009;3:453−455.

[3] Jankus V., Data P., Graves D., McGuinness C., Santos J., Bryce M. R., Dias F. B., Monkman A.P. Highly Efficient TADF OLEDs: How The Emitter−Host Interaction Controls Both

the Excited State Species and Electrical Properties of the Devices to Achieve Near 100% Triplet Harvesting and High Efficiency. Adv. Funct. Mater. 2014;24:6178−6186.

[4] Adachi C., Baldo M. A., Thompson M. E., Forrest S. R. J. Appl. Phys. 2001;90:5048–5051.

[5] Lin T.-A., Chatterjee T., Tsai W.-L., Lee W.-K., Wu M.-J., Jiao M., Pan K.-C., Yi C.-L., Chung C.-L., Wong K.-T., Wu. C.-C. Sky-Blue Organic Light Emitting Diode with 37% External Quantum Efficiency Using Thermally Activated Delayed Fluorescence from Spiroacridine-Triazine Hybrid. Adv. Mater. 2016;28:6976−6983.

[6] Kaji H., Suzuki H., Fukushima T., Shizu K., Suzuki K., Kubo S., Komino T., Oiwa H., Suzuki F., Wakamiya A., Murata Y., Adachi. C. Purely Organic Electroluminescent Material Realizing 100% Conversion from Electricity to Light. Nat.Comm. 2015;6:8476 1−8.

[7] Uoyama, H., Goushi, K., Shizu, K., Nomura, H., Adachi, C. Highly Efficient Organic Light-Emitting Diodes from Delayed Fluorescence. Nature 2012;492:234−238.

[8] Lee, S.Y., Adachi, C., Yasuda. T. High-Efficiency Blue Organic Light-Emitting Diodes Based on Thermally Activated Delayed Fluorescence from Phenoxaphosphine and Phenoxathiin Derivatives. Adv. Mater. 2016;28:4626–4631.

[9] Hung W.-Y., Fang G.-C., Lin S.-W., Cheng S.-H., Wong K.-T., Kuo T.-Y., Chou. P.-T. The First Tandem All-exciplex-based WOLED. Sci. Rep. 2014;4:5161–5167.

[10] Michaleviciute A., Gurskyte E., Volyniuk D.Yu., Cherpak V.V., Sini G., Stakhira P.Y., Grazulevicius. J.V. Star-Shaped Carbazole Derivatives for Bilayer White Organic Light-Emitting Diodes Combining Emission from Both Excitons and Exciplexes. J. Phys. Chem. C 2012;116:20769−20778.

[11] Kim K.-H., Yoo S.-J., Kim J.-J. Boosting Triplet Harvest by Reducing Non-radiative Transition of Exciplex Toward Fluorescent Organic Light-emitting Diodes with 100% Internal Quantum Efficiency Chem. Mater. 2016;28:1936–1941.

[12] Lee J.-H., Cheng S.-H., Yoo S.-J., Shin H., Chang J.-H., Wu C.-I., Wong K.-T., Kim. J.-J. An Exciplex Forming Host for Highly Efficient Blue Organic Light Emitting Diodes with Low Driving Voltage. Adv. Mater. 2015;25:361–366.

[13] Shin H., Lee S., Kim K.-H., Moon C.-K., Yoo S.-J., Lee J.-H., Kim J.-J. Blue Phosphorescent Organic Light-Emitting Diodes Using an Exciplex Forming Co-Host with the External Quantum Effi ciency of Theoretical Limit. Adv. Mater. 2014;26:4730–4734.

[14] Cherpak V., Stakhira P., Minaev B., Baryshnikov G., Stromylo E., Helzhynskyy I., Chapran M., Volyniuk D., Tomkute-Luksiene D., Malinauskas T. et al. Efficient "Warm-White" OLEDs Based on the Phosphorescent Bis-2-Cyclometalated Iridium[III]Complex. J. Phys. Chem. C 2014;118:11271−11278.

[15] Kalinowski J. Excimers and Exciplexes in Organic Electroluminescence. Mater. Sci.-Pol. 2009;27:735−756.

[16] Hung W.-Y., Fang G.-C., Chang Y.-C., Kuo T.-Y., Chou P.-T., Lin S.-W., Wong. K.-T. Highly Efficient Bilayer Interface Exciplex For Yellow Organic LightEmitting Diode. ACS Appl. Mater. Interfaces 2013;5:6826−6831.

[17] Liu X.-K., Chen Z., Zheng C.-J., Liu C.-L., Lee C.-S., Li F., Ou X.-M., Zhang. X.-H. Prediction and Design of Efficient Exciplex Emitters for High-Efficiency, Thermally Activated Delayed-Fluorescence Organic Light-Emitting Diodes. Adv. Mater. 2015;28:2378–2383.

[18] Cherpak V., Gassmann A., Stakhira P., Volyniuk D., Grazulevicius J.V., Michaleviciute A., Tomkeviciene A., Barylo G., von Seggern H. Three-Terminal Light-Emitting Device with Adjustable Emission Color Org. Electron. 2014;15:1396–1400.

[19] Chen D., Liu K., Gan L., Liu M., Gao K., Xie G., Ma Y., Cao Y., Su. S.-J. Modulation of Exciton Generation in Organic Active Planar pn Heterojunction: Toward Low Driving Voltage and

High-Efficiency OLEDs Employing Conventional and Thermally Activated Delayed Fluorescent Emitters. Adv. Mater. 2016;28:6758–6765.

[20] Zhang D., Cai M., Zhang Y., Bin Z., Zhang D., Duan. L. Simultaneous Enhancement of Efficiency and Stability of Phosphorescent OLEDs Based on Efficient Förster Energy Transfer from Interface Exciplex. ACS Appl. Mater. Interfaces 2016;8:3825–3832.

[21] Chapran M., Ivaniuk K., Stakhira P., Cherpak V., Hotra Z., Volyniuk D., Michaleviciute A., Tomkeviciene A., Voznyak L., Grazulevicius. J.V. Essential Electro-Optical Differences of Exciplex Type OLEDs Based on a Starburst Carbazole Derivative Prepared by Layer-By-Layer and Codeposition Processes. Synth. Met. 2015;209:173–177.

[22] Hung W.-Y., Chiang P.-Y., Lin S.-W., Tang W.-C., Chen Y.-T., Liu S.-H., Chou P.-Ta., Hung Y.-T., Wong. K.-T. Balance the Carrier Mobility to Achieve High Performance Exciplex OLED Using a New Triazine-Based Acceptor. ACS Appl. Mater. Interfaces 2016;8:4811–4818.

[23] Tsai T.-C., Hung W.-Y., Chi L.-C., Wong K.-T., Hsieh C.-C., Chou P.-T. A. New Ambipolar Blue Emitter for NTSC Standard Blue Organic Light-Emitting Device. Org. Electron. 2009;10:158 − 162.

[24] Miyamoto E., Yamaguchi Y., Yokoyama M. Electrophotography 1989;28:364–370.

[25] Kukhta N.A., Volyniuk D., Peciulyte L., Ostrauskaite J., Juska G., Grazulevicius J.V. Structure-Property Relationships of Star-Shaped Blue-Emitting Charge-Transporting 1,3,5-Triphenylbenzene Derivatives Dyes. Pigm. 2015;117:122–132.

[26] Amorim C.A., Cavallari M.R., Santos G., Fonseca F.J., Andrade A.M., Mergulhão S. Determination of Carrier Mobility in MEH-PPV Thin-Films by Stationary and Transient Current Techniques. J. Non-Cryst. Solids 2012;358:484–491.

[27] Reghu R.R., Grazulevicius J.V., Simokaitiene J., Miasojedovas A., Kazlauskas K., Jursenas S., Data P., Karon K., Lapkowski M., Gaidelis V., Jankauskas V. Glass-Forming Carbazolyl and Phenothiazinyl Tetra Substituted Pyrene Derivatives: Photophysical, Electrochemical, and Photoelectrical Properties J. Phys. Chem. C 2012;116:15878−15887.

[28] Juska G., Genevicius K., Viliunas M., Arlauskas K., Stuchlõkova H., Fejfar A., Kocka J. New Method of Drift Mobility Evaluation in μc-SI:H, Basic Idea and Comparison with Time-of-Light. J. Non-Cryst. Solids 2000;266-269:331−335.

[29] Mimaite V., Grazulevicius J. V., Laurinaviciute R., Volyniuk D., Jankauskas V., Sini G. Can Hydrogen Bonds Improve the Hole-Mobility in Amorphous Organic Semiconductors? Experimental and Theoretical Insights. J. Mater. Chem. C. 2015;3:11660−11674.

[30] Greenham N., Friend R., Bradley D. Measuring the Efficiency of Organic Light-Emitting Devices. Adv. Mater. 1994;6:491–494.

[31] Angioni E., Chapran M., Ivaniuk K., Kostiv N., Cherpak V., Stakhira P., Lazauskas A., Tamulevicius S., Volyniuk D., Findlay N. J., Tuttle T., Grazulevicius J.V., Skabara. P.J. A Single Emitting Layer White OLED Based on Exciplex Interface Emission. J. Mater. Chem. C 2016;4:3851–3856.

[32] Tucker S. H. J. Iodination in the carbazole series. Chem. Soc. 1926;1:546–553.

[33] Grigalevicius S., Tsai M. H., Grazulevicius Wu C. C. Well defined carbazol-39-diyl based oligomers with diphenylamino end-cap as novel amorphous molecular materials for optoelectronics. J. Photochem. Photobiol. A: Chem. 2005;174:125–129.

[34] Lux M., Strohriegl P., Hoecker H. Polymers with Pendant Carbazolyl Groups, 2. Synthesis and Characterization of Some Novel Liquid Crystalline Polysiloxanes. Macromol. Chem. 1987;188:811–820.

[35] Limburg W. W., Yanus J. F., Williams D. J., Goedde A.O., Pearson J. M. Anionic Polymerization of n-Ethyl-2-Vinylcarbazole and n-Ethyl-3-Vinylcarbazole. J. Polym. Sci. Polym. Chem. Ed. 1975;13:1133–1139.

[36] Dierschke F., Grimsdale A.C., Mullen K. Efficient Synthesis of 2,7-Dibromocarbazoles as Components for Electroactive Materials. Synthesis 2003:2470–2472.

[37] Patrick D.A., Boykin D.W., Wilson W.D., Tanious F.A., Spychalaz J., Bender B.C., Hall J.E., Dykstra C.C., Ohemeng K.A., Tidwell R.R. Anti-Pneumocystis Carinii Pneumonia Activity of Dicationic Carbazoles. Eur. J. Med. Chem. 1997;32:781–793.

[38] Guerra W. D., Rossi R. A., Pierini A. B., Barolo S. M. Transition-Metal-Free" Synthesis of Carbazoles by Photostimulated Reactions of 2′-Halo[1,1′-Biphenyl]-2-Amines. J. Org. Chem. 2015;80:928–941.

[39] SPARTAN'14 for Windows Version 1.1.4. 1840 Von Karman Avenue, Suite 370, Irvine, CA 92612: Wavefunction, Inc., 2013.

[40] Sun J., Jiang H.-J., Jin-Long Zh., Tao Y., Chen R.-F. Synthesis and Characterization of Heteroatom Substituted Carbazole Derivatives: Potential Host Materials for Phosphorescent Organic Light-Emitting Diodes. New J. Chem. 2013;37:977–985.

[41] Mei J., Leung N.L.C., Kwok R.T.K., Lam J.W.Y., Tang. B.Z. Aggregation-Induced Emission: Together We Shine, United We Soar! Chem. Rev. 2015;115:11718–11941.

[42] Zhang Q., Li B., Huang S., Nomura1 H., Tanaka H., Adachi. C. Efficient Blue Organic Light-Emitting Diodes Employing Thermally Activated Delayed Fluorescence. Nat. Photonics 2014;8:326–332.

[43] Baldo M.A., Adachi C., Forrest. S.R. Transient Analysis of Organic Electrophosphorescence. II. Transient Analysis of Triplet-Triplet Annihilation. Phys. Rev. B. 2000;62:967–10 977.

[44] Comision internationale de l'eclairage international commision on illiumination internationale beleuchtungskommission. Technical report colorimetry second edition. CIE 15.2. 1986:1–74,

[45] Ambrose J.F., Nelson R.F. J. Anodic Oxidation Pathways of Carbazoles. I. Carbazole and N-Substituted Derivatives. Electrochem. Soc. 1968;115:1159–1164.

[46] Qu J., Suzuki Y., Shiotsuki M., Sanda F., Masuda T. Synthesis and Electro-Optical Properties f oHelical Polyacetylenes Carrying Carbazole and Triphenylamine Moieties. Polymer 2007;48:4628–4636.

[47] Reig M., Puigdollers J., Velasco. D. Molecular Order of Air-Stable p-Type Organic Thin- Film Transistors by Tuning the Extension of the Pconjugated Core: The Cases of Indolo[32-b]- Carbazole and Triindole Semiconductors. J. Mater. Chem. C 2015;3:506–513.

[48] Jou J.-H., Sahoo S., Kumar S., Yu H.-H., Fang P.–H., Singh M.,Krucaite G., Volyniuk D., Grazulevicius J.V.,Grigalevicius. S. A Wet- and Dry-Process Feasible Carbazole Type Host for Highly Efficient Phosphorescent OLEDs. J. Mater. Chem. C 2015;3:12297–12307.

[49] Chang C.-H., Griniene R., Su Y.-D., Yeh C.-C., Kao H.-C., Grazulevicius J.V., Volyniuk D., Grigalevicius. S. Efficient Red Phosphorescent OLEDs Employing Carbazole-Based Materials as the Emitting Host. Dyes and Pigments 2015;122:257–263.

[50] Xie F.X., Choy W.C.H., Wang C.D., Li X.C., Zhang S.Q., Hou J.H. Low Temperature Solution-Processed Hydrogen Molybdenum and Vanadium Bronzes for an Efficient Hole-Transport Layer in Organic Electronics. Adv. Mater. 2013;25:2051–2055.

[51] T.W. Ng, M.F. Lo, M.K. Fung, W.J. Zhang, C.S. Lee, Charge-Transfer Complexes and Their Role in Exciplex Emission and Near-Infrared Photovoltaics. Adv. Mater. 26 (2014) 5569–5574.

[52] Zang T., Chu B., Li W., Su Z., Peng Q.M., Zhao B., Luo Y., Jin F., Yan X., Gao Y., Wu H., Zhang F., Fan D., Wang J. Efficient Triplet Application in Exciplex Delayed fluorescence Oleds

Using a Reverse Intersystem Crossing Mechanism Based on a ΔE_{S-T} of Around Zero, ACS Appl. Mater. Interfaces 2014;6:11907–11914.

[53] Cherpak V., Stakhira P., Minaev B., Baryshnikov G., Stromylo E., Helzhynskyy I., Chapran M., Volyniuk D., Hotra Z., Dabuliene A., Tomkeviciene A., Voznyak L., Grazulevicius. J.V. Mixing of Phosphorescent and Exciplex Emission in Efficient Organic Electroluminescent Devices. ACS Appl. Mater. Interfaces 2015;7:1219−1225.

[54] T. Deksnys, J. Simokaitiene, J. Keruckas, D. Volyniuk, O. Bezvikonnyi, V. Cherpak, P. Stakhira, K. Ivaniuk, I.r Helzhynskyy, G. Baryshnikov, B. Minaev, J.V. Grazulevicius. New J. Chem., 2017; doi: 10.1039/C6NJ02865A.

[55] Jankus V., Chiang C.-J., Dias F., Monkman A.P. Deep Blue Exciplex Organic Light-Emitting Diodes with Enhanced Efficiency, P-type or E-type Triplet Conversion to Singlet Excitons? Adv. Mater. 2013;25:1455−1459.

[56] Goushi K., Yoshida K., Sato K., Adachi C. Organic light-emitting diodes employing efficient reverse intersystem crossing for triplet-to-singlet state conversion. Nature Photonics 2012;6:253–258.

[57] Jou J.-H., Kumar S., Agrawal A., Li Ts.-H., Sahoo S. Approaches for Fabricating High Efficiency Organic Light Emitting Diodes. J. Mater. Chem. C 2015;3:2974−3002.

[58] Huang J., Su J.-H., Tian H. The development of anthracene derivatives for organic light-emitting diodes J. Mater. Chem. 2012;22:10977−10989.

[59] Guo Z., Zhu W., Tian H. Dicyanomethylene-4H-pyran chromophores for OLED emitters, logic gates and optical chemosensors. Chem. Commun. 2012;48:6073–6084.